Integrity-Aware Marine Navigation under Multi-Sensor Attacks Using Adaptive Descriptor Error-State Filtering

Mohammadreza Nematollahi[1], Mahdi Taheri[2], Shahab Chehraghi[1], Khashayar Khorasani[1]

Abstract— **This paper develops a marine positioning, navigation, and timing (PNT) estimator for coordinated sensor-integrity attacks targeting inertial measurement unit (IMU), magnetometer, and GNSS position measurements. The estimator places a descriptor unknown-input update inside a loosely coupled error-state navigation filter, so IMU-induced unknown-input components are suppressed at the correction step without augmenting the navigation error state. A separate bias-estimation layer is then combined with per-axis fading-memory covariance learning to track nonstationary integrity-loss terms in the GNSS position and magnetometer channels. Simulations on a Marine Systems Simulator (MSS) surface-vessel model show that the adaptive covariance layer improves integrity-loss tracking and attitude estimation while maintaining comparable position accuracy relative to a non-adaptive two-stage baseline in the considered multi-sensor attack case.**

I. Introduction

Autonomous marine platforms rely on positioning, navigation, and timing (PNT) estimates as operational inputs, not only as display quantities. In integrated bridge systems (IBS), these estimates are fed directly to guidance, collision-avoidance, and motion-planning modules [1]. A corruption in the navigation solution can therefore propagate through the autonomy stack, creating a cyber-physical safety hazard rather than a purely informational error [2].

Shipboard navigation typically fuses GNSS, inertial sensing, and magnetic heading data via stochastic filtering or graph-based fusion [3], and, despite the maturity of the filtering, the security assumptions underlying this fusion are fragile. Much of the available protection is centered on GNSS spoofing and interference [4], whereas attacks on the inertial and magnetic channels remain equally consequential for closed-loop operation. These sensors drive the high-rate propagation and attitude-reference mechanisms; injected signals at those channels can corrupt short-time vessel motion estimates and defeat cross-checks that depend on inertial consistency [5], [6].

Existing work has begun to address the integrity of IMU and magnetometer data by employing recovery architectures that reject compromised updates and reconstruct attitude estimates from auxiliary measurements [7]. In these approaches, estimates from one sensor stream are used to build a virtual equivalent of the sensor for other compromised sensors, thereby sustaining operation under adversarial injections [8]. In parallel, the fault-diagnosis literature widely employs two-stage Kalman structures to estimate IMU faults and biases with reduced complexity [9]. Still, these formulations typically assume structured fault models and are not designed for unmodeled, nonstationary adversarial injections. Moreover, these works primarily emphasize fault detection rather than resilient estimation and are not primarily designed to maintain accurate state estimates under persistent adversarial compromise.

Motivated by these limitations, this paper proposes a loosely coupled error-state Kalman filter (ESKF) for marine navigation in the presence of IMU corruption, magnetic-channel integrity loss, and GNSS position bias. The filter embeds an unknown-input (UI) correction within an adaptive two-stage filtering scheme. The UI part limits the extent to which the filter can be driven by the unknown IMU attack channel. The adaptive two-stage scheme then interprets GNSS position and magnetometer corruptions as non-stationary, bias-like variables and learns their per-axis drive covariances from parity-space covariance and lag-correlation statistics. The proposed loosely coupled architecture preserves compatibility with standard INS/GNSS architectures while adding integrity adaptation at the inertial and magnetic sensing layers. The main contributions of the paper are as follows:

- We integrate a two-stage unknown-input update, following the descriptor formulation in [10], into a loosely coupled error-state navigation filter with the standard update-reset-propagate loop. The resulting estimator reduces the sensitivity of the measurement update to compromised IMU samples while avoiding explicit augmentation of the navigation error state.
- We develop a per-axis covariance-adaptation scheme for time-varying integrity loss in the GNSS position and magnetometer channels. The update is driven by covariance matching and lagged-correlation diagnostics in a parity-projected residual space, together with activation- and coherence-aware regularization that promotes conservative adaptation under weak excitation and near-collinearity, thereby stabilizing covariance learning for weakly identifiable magnetometer directions.

[1]Mohammadreza Nematollahi (m_nemato@encs.concordia.ca), Shahab Chehraghi (s_chehra@encs.concordia.ca), and Khashayar Khorasani (kash@ece.concordia.ca) are with the Department of Electrical and Computer Engineering, Concordia University, Montreal, Canada.

[2] Mahdi Taheri (mtaheri@caltech.edu) is with the Graduate Aerospace Laboratories of the California Institute of Technology (GALCIT), Pasadena, CA, USA.

K. Khorasani acknowledges support from the Natural Sciences and Engineering Research Council of Canada (NSERC) and the Department of National Defence (DND) through the Discovery Grant and DND Supplemental Programs. This work was also supported in part by DND's Innovation for Defence Excellence and Security (IDEaS) program. The opinions and conclusions are solely those of the authors and do not represent or imply endorsement by IDEaS, DND, or the Government of Canada.

The remainder of the paper is organized as follows. Section II introduces the notation used in the paper and formalizes the measurement models and the adopted false-data-injection (FDI) cyber-attack abstractions. Section III presents vessel ECEF inertial navigation kinematics and derives the associated error-state model. Section IV develops the proposed resilient, loosely coupled error-state navigation filter. Section V reports simulation results demonstrating the resilience improvement achieved by the proposed solution. Section VI concludes the paper.

II. Notation and Measurement Models

A. Notation

Throughout this paper, the indices or superscripts $\{e\}$, $\{i\}$, and $\{b\}$ denote the ECEF, ECI, and body frames, with $\{b\}$ coincident with the IMU frame. The vessel translational states are $r^e_{eb}, v^e_{eb} \in \mathbb{R}^3$, and the attitude is $R^e_b \in \mathbb{SO}(3)$ with $R^b_e = (R^e_b)^\top$. The IMU specific forces and angular rate measurements are denoted by $f^b, \omega^b_{ib} \in \mathbb{R}^3$, and $\omega^e_{ie} \in \mathbb{R}^3$ denotes the (constant) Earth rotation vector in ECEF. The effective gravity, including the gravitational acceleration and centrifugal acceleration, is denoted by $g^e(r^e_{eb}) \in \mathbb{R}^3$, and $B_e(r^e_{eb}) \in \mathbb{R}^3$ denotes the Earth's magnetic field in ECEF. For $a \in \mathbb{R}^3$, $S(a) \in \mathbb{R}^{3\times 3}$ is the skew operator satisfying $S(a)^\top = -S(a)$ and $S(a)b = a \times b$, where $(\cdot)^\vee$ denotes its inverse, i.e., $(S(a))^\vee = a$. Finally, $\mathcal{N}(\mu, \Sigma)$ denotes a Gaussian distribution with mean μ and covariance Σ.

B. Sensor Measurement Models and Cyber-Attack Models

After calibration, the IMU outputs sampled measurements of specific force and angular rate. At the same time, the tri-axial magnetometer measures the local magnetic field vector expressed in the body frame being used for attitude estimation. Moreover, in loosely coupled INS/GNSS integration models, we have access to processed GNSS measurements of the vessel's position and velocity in the ECEF frame. Finally, an inclinometer provides the direction of the effective gravity vector expressed in the body frame, which can be used to estimate vessel tilt and to condition the magnetometer compass.

Sensor-integrity compromises are modeled as additive, time-varying terms in the IMU, magnetometer, and GNSS position outputs [4], [11]–[13]. The attacked measurement models are

$$
\begin{aligned}
\tilde{f}^b[k] &= f^b[k] + a_a[k] + n_a[k],\\
\tilde{\omega}^b_{ib}[k] &= \omega^b_{ib}[k] + a_g[k] + n_g[k],\\
z_r[k] &= r^e_{eb}[k] + a_r[k] + n_r[k],\\
z_v[k] &= v^e_{eb}[k] + n_v[k],\\
\tilde{B}_b[k] &= R^b_e[k] B_e(r^e_{eb}[k]) + a_m[k] + n_m[k],\\
u^b_g[k] &\triangleq \frac{R^b_e[k]\, g^e\big(r^e_{eb}[k]\big)}{\|R^b_e[k]\, g^e\big(r^e_{eb}[k]\big)\|} + n_{in}[k].
\end{aligned}
\tag{1}
$$

where $n_a[k] \sim \mathcal{N}(0, R_a)$, $n_g[k] \sim \mathcal{N}(0, R_g)$, $n_r[k] \sim \mathcal{N}(0, R_r)$, $n_v[k] \sim \mathcal{N}(0, R_v)$, $n_m[k] \sim \mathcal{N}(0, R_m)$, and $n_{in}[k] \sim \mathcal{N}(0, R_{in})$, with R_{in} denoting the inclinometer gravity-direction noise covariance. The terms $a_a[k]$, $a_g[k]$, $a_r[k]$, and $a_m[k]$ denote adversarial injections in the specific-force, angular-rate, GNSS-position, and magnetometer channels, respectively.

We do not assume an *a priori* parametric model for IMU injections, but for magnetometer and GNSS position measurements, we impose random-walk *a priori* models with time-varying unknown covariances

$$
\begin{aligned}
a_r[k+1] &= a_r[k] + w_r[k]\\
a_m[k+1] &= a_m[k] + w_m[k],
\end{aligned}
\tag{2}
$$

where $w_r[k], w_m[k]$ are zero-mean stochastic inputs with unknown *time-varying* covariances $Q_{a_r}[k], Q_{a_m}[k]$.

***Remark** 2.1:* The random-walk dynamics in (2) for (a_r, a_m) are adopted as an estimator-side prior that regularizes online tracking of nonstationary integrity loss, where the unknown drive covariances $Q_{a_r}[k]$ and $Q_{a_m}[k]$ capture the time-variation rate of these corruptions and are adapted online. Calibration errors and benign non-stationarities can also be absorbed into the same integrity-loss terms, but the focus here is on the resilience of the navigation solution rather than on distinguishing among the sources of error.

III. Marine Vessel ECEF INS Kinematics and Error-State Model

A. Nonlinear ECEF Kinematics and Error Dynamics

We describe the vessel kinematics in ECEF to remain consistent with GNSS aiding and to avoid long-range frame effects. The continuous-time ECEF dynamics are

$$
\begin{aligned}
\dot{r}^e_{eb} &= v^e_{eb},\\
\dot{v}^e_{eb} &= R^e_b f^b + g^e(r^e_{eb}) - 2S(\omega^e_{ie}) v^e_{eb},\\
\dot{R}^e_b &= R^e_b S(\omega^b_{ib}) - S(\omega^e_{ie}) R^e_b.
\end{aligned}
\tag{3}
$$

The nominal estimator propagates the state using the compromised IMU measurements $(\tilde{f}^b, \tilde{\omega}^b_{ib})$ as

$$
\begin{aligned}
\dot{\hat{r}}^e_{eb} &= \hat{v}^e_{eb},\\
\dot{\hat{v}}^e_{eb} &= \hat{R}^e_b \tilde{f}^b + g^e(\hat{r}^e_{eb}) - 2S(\omega^e_{ie}) \hat{v}^e_{eb},\\
\dot{\hat{R}}^e_b &= \hat{R}^e_b S(\tilde{\omega}^b_{ib}) - S(\omega^e_{ie}) \hat{R}^e_b,
\end{aligned}
\tag{4}
$$

Define the translational errors and the right-invariant attitude error as

$$
\delta r = r^e_{eb} - \hat{r}^e_{eb}, \delta v = v^e_{eb} - \hat{v}^e_{eb}, \delta R = R^e_b (\hat{R}^e_b)^\top \in \mathbb{SO}(3). \tag{5}
$$

The mean-value error dynamics are

$$
\begin{aligned}
&\delta\dot{r} = \delta v,\\
&\delta\dot{v} = (\delta R - I)\hat{R}^e_b \tilde{f}^b + \Upsilon(\hat{r}^e_{eb}, \delta r) - 2S(\omega^e_{ie})\delta v - \delta R \hat{R}^e_b a_a,\\
&\dot{\delta R} = -S(\omega^e_{ie})\delta R + \delta R S(\omega^e_{ie}) - \delta R S\big(\hat{R}^e_b a_g\big),
\end{aligned}
\tag{6}
$$

where $\Upsilon(\hat{r}^e_{eb}, \delta r) = g^e(\hat{r}^e_{eb} + \delta r) - g^e(\hat{r}^e_{eb})$.

B. Linearized ECEF Error-State Model

Let $\zeta \in \mathbb{R}^3$ be the Lie-log attitude error coordinate $\zeta = -(\log(\delta R))^\vee, \delta R = \exp(-S(\zeta))$, with the principal matrix logarithm (single-valued for angles in $[0, \pi)$). To linearize (6) about the origin using ζ as the attitude error state, define

$$
\delta x = [\zeta^\top, \delta v^\top, \delta r^\top]^\top \in \mathbb{R}^9, \; d(t) = [a_a^\top, a_g^\top]^\top \in \mathbb{R}^6, \tag{7}
$$

to obtain the LTV error model

$$
\delta\dot{x} = F(t)\delta x + G(t) d(t), \tag{8}
$$

where

$$F(t)=\begin{bmatrix}-S(\omega_{ie}^{e}) & 0 & 0\\ S(\hat{R}_b^e\tilde{f}^b) & -2S(\omega_{ie}^{e}) & G_g(\hat{r}_{eb}^{e})\\ 0 & I & 0\end{bmatrix},\qquad G(t)=\begin{bmatrix}0 & \hat{R}_b^e\\ -\hat{R}_b^e & 0\\ 0 & 0\end{bmatrix}. \tag{9}$$

This follows from $\delta R \approx I - S(\zeta)$, $\dot{\delta R} \approx -S(\dot{\zeta})$, and $\Upsilon(\hat{r}_{eb}^{e},\delta r)\approx G_g(\hat{r}_{eb}^{e})\delta r$ with $G_g(\hat{r}_{eb}^{e})$ calculated numerically.

C. Discrete-Time Error-State Model

With IMU sampling period $T_s>0$, discretization of (8) over $[t_{k-1},t_k)$, $t_k=t_{k-1}+T_s$, yields

$$\delta x[k]=\Phi[k-1]\delta x[k-1]+\Gamma[k-1]d[k-1], \tag{10}$$

where $\delta x[k]=\delta x(t_k)$ and $d[k]=d(t_k)$. Over each interval $t\in[t_{k-1},t_k)$, we use $F[k]=F(t_{k-1}+\frac{T_s}{2}), G[k]=G(t_{k-1}+\frac{T_s}{2})$, so that

$$\Phi[k]=\exp(F[k]T_s),\quad \Gamma[k]=\int_0^{T_s}\exp(F[k]\tau)\,G[k]\,d\tau, \tag{11}$$

which can be computed using the approach in [14].

D. Linearized Residual Models

The stacked linear residual model is now

$$y[k]=H[k]\delta x[k]+D[k]b[k]+n[k], \tag{12}$$

where $n[k]\sim\mathcal{N}(0,R[k])$, $R[k]=\mathrm{blkdiag}(R_r,R_v,R_m,R_{in})$, and $b[k]=[a_r^\top[k],a_m^\top[k]]^\top\in\mathbb{R}^6$. We have

$$y[k]=\begin{bmatrix}y_r[k]\\ y_v[k]\\ y_B[k]\\ y_{\mathrm{att}}[k]\end{bmatrix}=\begin{bmatrix}\delta r[k]+a_r[k]\\ \delta v[k]\\ H_m[k]\delta x[k]+a_m[k]\\ H_{\mathrm{att}}[k]\delta x[k]\end{bmatrix}, D[k]=\begin{bmatrix}I_3 & 0\\ 0 & 0\\ 0 & I_3\\ 0 & 0\end{bmatrix} \tag{13}$$

that gives $H[k]=[H_r^\top[k],H_v^\top[k],H_m^\top[k],H_{\mathrm{att}}^\top[k]]^\top$, with

$$\begin{aligned}H_r[k]&=\begin{bmatrix}0_{3\times3} & 0_{3\times3} & I_3\end{bmatrix},\\ H_v[k]&=\begin{bmatrix}0_{3\times3} & I_3 & 0_{3\times3}\end{bmatrix},\\ H_m[k]&=\begin{bmatrix}-\hat{R}_e^b[k]\,S\big(B_e(\hat{r}_{eb}^{e}[k])\big) & 0_{3\times3} & \hat{R}_e^b[k]\,J_B[k]\end{bmatrix},\end{aligned} \tag{14}$$

with $J_B[k]=\frac{\partial B_e(r)}{\partial r}\big|_{r=\hat{r}_{eb}^{e}[k]}\in\mathbb{R}^{3\times3}$ calculated numerically, and

$$\begin{aligned}H_{\mathrm{att}}[k]&=\begin{bmatrix}H_{\mathrm{att},\zeta}[k] & 0_{3\times3} & H_{\mathrm{att},r}[k]\end{bmatrix},\\ H_{\mathrm{att},\zeta}[k]&=-\frac{1}{\|\hat{g}^b[k]\|}\Big(I_3-\hat{u}_g^b[k]\hat{u}_g^b[k]^\top\Big)\hat{R}_e^b[k]\,S\big(\hat{g}^e[k]\big),\\ H_{\mathrm{att},r}[k]&=\frac{1}{\|\hat{g}^b[k]\|}\Big(I_3-\hat{u}_g^b[k]\hat{u}_g^b[k]^\top\Big)\hat{R}_e^b[k]\,G_g\big(\hat{r}_{eb}^{e}[k]\big).\end{aligned} \tag{15}$$

where $\hat{g}^b[k]=\hat{R}_e^b[k]\,g^e\big(\hat{r}_{eb}^{e}[k]\big)$.

IV. Descriptor Error-State Filter with Adaptive Integrity-Loss Learning

Algorithm 1 summarizes the proposed adaptive two-stage unknown-input error-state Kalman filter. It implements the two-stage descriptor idea of [10] within an error-state update-reset-propagate navigation architecture, while extending the second stage by adapting the bias-drive covariance associated with the bias variable, which represents unstructured integrity loss rather than a stationary sensor bias.

Following [10], [15], we maintain the bias-free decomposition $\delta x[k]=\delta x^{\mathrm{bf}}[k]+\beta[k]\,b[k]$. The coupling matrix $\beta[k]$ is defined by the compressed cross-covariance relation $P^{\delta xb}[k]=\beta[k]\,P^{bb}[k]$, so that the total covariance and $(\delta x^{\mathrm{bf}},b)$ are then estimated in two coupled stages without explicitly augmenting the navigation error state. The prediction step, i.e., Algorithm 1(A), propagates $(\hat{x}^{\mathrm{bf},-},P^{\mathrm{bf},-})$, $(\hat{b}^-,P^{bb,-})$, and β^- using (Φ,Γ,Q_x). Here, Q_x is computed from $R_{\mathrm{imu}}=\mathrm{blkdiag}(R_a,R_g)$, while $Q_b[k]=\mathrm{blkdiag}(Q_{a_r}[k],Q_{a_m}[k])$ denotes the time-varying bias covariance.

The goal of Stage I, i.e., Algorithm 1(B), is to avoid using prediction information along components of δx that are reachable from the unknown-input channel over the last step $\Gamma[k-1]d[k-1]$. This is enforced by selecting the matrix $E[k]$ as a basis of the left null-space of $\Gamma[k-1]$, and using the subroutine “DescInfoUpdate” to perform a constrained information-form update on δx^{bf}, with:

$$J_x[k]=E[k]^\top\big(E[k]P^{\mathrm{bf},-}[k]E[k]^\top\big)^{-1}E[k]+H[k]^\top R[k]^{-1}H[k]. \tag{16}$$

Then $P^{\mathrm{bf},+}[k]=J_x[k]^{-1}$ and $K_x[k]=P^{\mathrm{bf},+}[k]H[k]^\top R[k]^{-1}$, and the bias-free estimate is updated using the innovation $y^{\mathrm{bf}}[k]=y[k]-H[k]\hat{x}^{\mathrm{bf},-}[k]$ as $\hat{x}^{\mathrm{bf},+}[k]=\hat{x}^{\mathrm{bf},-}[k]+K_x[k]y^{\mathrm{bf}}[k]$.

Stage II in Algorithm 1(C) uses subroutine “BiasUpdate” to update $b[k]$. Let $H_b^-[k]$ and $H_b^+[k]$ denote the pre-update and post-update bias signatures in measurement space, and let $\beta^+[k]$ denote the updated coupling matrix. With innovation $r_b[k]=y^{\mathrm{bf}}[k]-H_b^-[k]\hat{b}^-[k]$, the bias update uses the asymmetric information form

$$J_b[k]=(P^{bb,-}[k])^{-1}+(H_b^-[k])^\top R[k]^{-1}H_b^+[k]. \tag{17}$$

Then $P^{bb,+}[k]=J_b[k]^{-1}$. Note that in finite precision, it is recommended to compute $J_b[k]$ using a symmetric factorization and, if needed, add a small diagonal jitter $\varepsilon_J I$ before inversion to preserve positive definiteness. Finally, $\hat{b}^+[k]=\hat{b}^-[k]+P^{bb,+}[k](H_b^+[k])^\top R[k]^{-1}r_b[k]$.

After the update, the correction is formed in Algorithm 1(D) and injected into the nominal solution in Algorithm 1(F). The corrected state is then propagated over $[k,k+1]$ in Algorithm 1(G) using the compromised IMU measurements and a single-step Dormand–Prince integration of (4), initialized at the injected state. The propagation is then followed by a midpoint linearization for calculating $(F[k],G[k])$, and discretization using subroutine “discFGQ” implementing [14] to obtain $(\Phi[k],\Gamma[k],Q_x[k])$ for the next epoch.

To comply with the error-state architecture, we apply a reset step as in Algorithm 1(F). Define the Jacobian $\mathscr{G}_k=\mathrm{blkdiag}(J_r(\hat{\zeta}[k]),I_3,I_3)$, where $J_r(\cdot)$ denotes the *right Jacobian* of SO(3) associated with the exponential map $\delta R=\exp(-S(\zeta))$, and we have for $\phi\in\mathbb{R}^3$ and $\theta=\|\phi\|$,

$$J_r(\phi)=I_3-\frac{1-\cos\theta}{\theta^2}S(\phi)+\frac{\theta-\sin\theta}{\theta^3}S(\phi)^2. \tag{18}$$

Under the error-state reset map $\delta x\leftarrow\mathscr{G}\,\delta x$, the two-stage variables are mapped consistently as $P^{\mathrm{bf}}[k]\leftarrow\mathscr{G}_kP^{\mathrm{bf},+}[k]\mathscr{G}_k^\top,\beta[k]\leftarrow\mathscr{G}_k\beta^+[k]$, while $\hat{b}[k]=\hat{b}^+[k]$ and $P^{bb}[k]=P^{bb,+}[k]$. Notably, in this reset step, we enforce the zero total-mean convention by storing $\hat{x}^{\mathrm{bf}}[k]=-\beta[k]\hat{b}[k]$, so that $\hat{x}^{\mathrm{bf}}[k]+\beta[k]\hat{b}[k]=0$ after the reset map. The above reset procedure is included in the “Reset” subroutine.

In this work, $b[k]$ represents nonstationary integrity loss, so its process covariance $Q_b[k]$ cannot be treated as fixed

Algorithm 1 Adaptive two-stage unknown-input ESKF

Require: At epoch k: $y[k], H[k], D[k], R[k]$, and from $[k-1,k]$: $\Phi[k-1], \Gamma[k-1], Q_x[k-1]$, stored $(\hat{x}^{\mathrm{bf}}, P^{\mathrm{bf}}, \hat{b}, P^{bb}, \beta, Q_b, \xi, \mathscr{S})[k-1]$, tuning constants $\Theta = [\varpi_v,\, L,\, \varpi_{\mathrm{fim}},\, \varepsilon_\rho,\, \varepsilon_\alpha,\, \alpha_\gamma,\, s_{\mathrm{thr}},\, q_{\mathrm{bar}},\, \mu_{\mathrm{white}},\, \kappa_0,\, \kappa_t,\, \kappa_{\mathrm{tie}}]$.

Ensure: $\hat{\delta} x[k], P^{xx}[k]$, updated $(\hat{b}, P^{bb}, \beta)[k]$, updated $Q_b[k]$ (applied at $k+1$), and stored $(\hat{x}^{\mathrm{bf}}, P^{\mathrm{bf}})[k]$ after reset.

for $k = 1,2,\ldots$ **do**

(A) Prediction (bias, coupling, bias-free state)

$\hat{b}^- \leftarrow \hat{b}[k-1], \quad P^{bb,-} \leftarrow P^{bb}[k-1] + Q_b[k-1]$

$\Pi[k] \leftarrow \Phi[k-1]\beta[k-1]$

$\beta^- \leftarrow \big(\Pi[k]P^{bb}[k-1]\big)\,(P^{bb,-})^{-1}$

$\hat{x}^{\mathrm{bf},-} \leftarrow \Phi[k-1]\hat{x}^{\mathrm{bf}}[k-1] + \Pi[k]\hat{b}[k-1] - \beta^-\hat{b}^-$

$P^{\mathrm{bf},-} \leftarrow \Phi[k-1]P^{\mathrm{bf}}[k-1]\Phi[k-1]^\top + Q_x[k-1] + \Pi[k]P^{bb}[k-1]\Pi[k]^\top - \beta^- P^{bb,-}(\beta^-)^\top$

(B) Stage I: descriptor information update

Choose $E[k]$ such that $E[k]\Gamma[k-1] = 0$

$(\hat{x}^{\mathrm{bf},+}, P^{\mathrm{bf},+}, K_x) \leftarrow \mathrm{DescInfoUpdate}(E[k], \hat{x}^{\mathrm{bf},-}, P^{\mathrm{bf},-}, y[k], H[k], R[k])$

(C) Stage II: coupling and bias update

$H_b^- \leftarrow D[k] + H[k]\beta^-$

$\beta^+ \leftarrow \beta^- - K_x H_b^-$

$H_b^+ \leftarrow D[k] + H[k]\beta^+$

$(\hat{b}^+, P^{bb,+}) \leftarrow \mathrm{BiasUpdate}(\hat{b}^-, P^{bb,-}, H_b^-, H_b^+, y[k], H[k], R[k], \hat{x}^{\mathrm{bf},-})$

(D) Total correction

$\hat{\delta} x[k] \leftarrow \hat{x}^{\mathrm{bf},+} + \beta^+\hat{b}^+$

$P^{xx}[k] \leftarrow P^{\mathrm{bf},+} + \beta^+ P^{bb,+}(\beta^+)^\top$

(E) Parity features and Q_b adaptation

$U_y[k] \leftarrow H[k]\Gamma[k-1]$, choose $N_{\mathrm{ui}}[k]$ such that $N_{\mathrm{ui}}[k]U_y[k] = 0$

$y^{\mathrm{bf}}[k] \leftarrow y[k] - H[k]\hat{x}^{\mathrm{bf},-}$

$r_b[k] \leftarrow y^{\mathrm{bf}}[k] - H_b^-[k]\hat{b}^-$

$\Sigma_{\mathrm{ui},0}[k] \leftarrow N_{\mathrm{ui}}[k](H[k]P^{\mathrm{bf},-}[k]H[k]^\top + R[k])N_{\mathrm{ui}}[k]^\top$,

$(e_{\mathrm{ui}}[k], D_b[k]) \leftarrow \mathrm{ParityWhiten}(N_{\mathrm{ui}}[k], r_b[k], \Sigma_{\mathrm{ui},0}[k], H_b^-[k])$

$(\mathscr{S}[k], \rho_{ij}[k]) \leftarrow \mathrm{UpdateGram}(\mathscr{S}[k-1], e_{\mathrm{ui}}[k], D_b[k], \Theta)$

$\gamma[k] \leftarrow \mathrm{SoftActivation}(\rho_{ij}[k], e_{\mathrm{ui}}[k], D_b[k], \Theta)$

$\xi[k] \leftarrow \mathrm{InflationOpt}(\xi[k-1], \gamma[k], \mathscr{S}[k], \rho_{ij}[k], D_b[k], \Theta)$

$Q_b[k] \leftarrow \mathrm{diag}(q_{\mathrm{bar}} \circ \exp(\xi[k]))$

(F) Injection and reset-map

Inject $\hat{\delta} x[k]$: $\hat{r}^+ \leftarrow \hat{r} + \hat{\delta} r$, $\hat{v}^+ \leftarrow \hat{v} + \hat{\delta} v$, $\hat{R}^+ \leftarrow \exp\big(-S(\hat{\zeta})\big)\hat{R}$

$(\hat{x}^{\mathrm{bf}}, P^{\mathrm{bf}}, \beta, \hat{b}, P^{bb})[k] \leftarrow \mathrm{Reset}(\hat{x}^{\mathrm{bf},+}, P^{\mathrm{bf},+}, \beta^+, \hat{b}^+, P^{bb,+}, \hat{\delta} x[k])$

(G) Propagation and discretization

Propagate corrected estimates to $k+1$

Form midpoint linearization $(F[k], G[k])$

$(\Phi[k], \Gamma[k], Q_x[k]) \leftarrow \mathrm{discFGQ}(F[k], G[k], R_{\mathrm{imu}})$

end for

and known. We therefore employ fading-memory covariance adaptation in the spirit of [16], but extend it to per-channel inflation factors rather than a single scalar. A key practical issue is the stable tuning of magnetometer-related components. Notably, their measurement signatures depend on the operating point and can become weakly excited or nearly collinear along typical trajectories, degrading the separability of bias directions and leading to unstable covariance updates or ambiguous bias attribution.

In particular, let $n_b = 6$, $\lambda[k] \in \mathbb{R}^{n_b}$ denote the per-axis inflation factors with $\lambda_i[k] \geq 1$, and define $\xi[k] = \log\lambda[k]$ and $\xi_{\mathrm{prev}} = \xi[k-1]$. The adapted diagonal bias covariance is then $Q_b[k] = \mathrm{diag}(q_{\mathrm{bar}} \circ \lambda[k])$ with baseline q_{bar}.

At each epoch k of the adaptation in Algorithm 1(E), a parity basis $N_{\mathrm{ui}}[k]$ is selected to annihilate the unknown-input signature in measurement space by using a basis of the left null space of $U_y[k] \triangleq H[k]\Gamma[k-1]$. Using the Stage II residual $r_b[k]$, we form the parity residual $r_{\mathrm{ui}}[k] = N_{\mathrm{ui}}[k]\, r_b[k]$ and call the "ParityWhiten" subroutine to compute the projected covariance as

$$\Sigma_{\mathrm{ui},0}[k] = N_{\mathrm{ui}}[k]\Big(H[k]P^{\mathrm{bf},-}[k]H[k]^\top + R[k]\Big)N_{\mathrm{ui}}[k]^\top, \quad (19)$$

and define

$$e_{\mathrm{ui}}[k] = \Sigma_{\mathrm{ui},0}[k]^{-1/2} r_{\mathrm{ui}}[k], D_b[k] = \Sigma_{\mathrm{ui},0}[k]^{-1/2} N_{\mathrm{ui}}[k] H_b^-[k]. \quad (20)$$

With these definitions, the covariance of parity innovations $e_{\mathrm{ui}}[k]$ admits the decomposed form

$$\Sigma_e(\xi) = I + D_b[k]\, P^{bb,-}(\xi)\, D_b[k]^\top, \quad (21)$$

where $P^{bb,-}(\xi) = P^{bb}[k-1] + Q_b(\xi)$ and $Q_b(\xi)$ denotes the candidate diagonal bias-drive covariance induced by ξ. From the parity innovations, with a chosen forgetting factor $\varpi_v \in (0,1)$ and lag depth $L \in \mathbb{Z}_{\geq 1}$, we maintain the exponentially weighted correlation statistics for $j = 1,\ldots,L$

$$\begin{aligned} C_0[k] &= \varpi_v C_0[k-1] + (1-\varpi_v) e_{\mathrm{ui}}[k] e_{\mathrm{ui}}[k]^\top, \\ C_j[k] &= \varpi_v C_j[k-1] + (1-\varpi_v) e_{\mathrm{ui}}[k] e_{\mathrm{ui}}[k-j]^\top. \end{aligned} \quad (22)$$

where $C_0[k]$ captures the innovation covariance, and $\{C_j[k]\}$ captures temporal correlation describing the deviation from whiteness in parity innovations.

The "UpdateGram" subroutine forms the instantaneous regression Gram matrix $D_b[k]^\top D_b[k]$ in the whitened parity space and updates its exponentially weighted accumulation by a forgetting factor $\varpi_{\mathrm{fim}} \in (0,1)$ as:

$$J_{\mathrm{acc}}[k] = \varpi_{\mathrm{fim}} J_{\mathrm{acc}}[k-1] + D_b[k]^\top D_b[k]. \quad (23)$$

Therefore, $\mathscr{S}[k]$ includes $J_{\mathrm{acc}}[k]$, $C_0[k]$, and $C_j[k]$. From $J_{\mathrm{acc}}[k]$ we form the pairwise coherence indicators as

$$\rho_{ij}[k] = \frac{|J_{\mathrm{acc}}[k]_{ij}|}{\sqrt{\max(J_{\mathrm{acc}}[k]_{ii} J_{\mathrm{acc}}[k]_{jj}, \varepsilon_\rho)}}. \quad (24)$$

A large $\rho_{ij}[k]$ indicates that directions i and j have been weakly separable in the observed parity space over the recent trajectory, a regime in which independent per-axis covariance adaptation becomes less reliable.

Next, given $(e_{\mathrm{ui}}[k], D_b[k])$, the SoftActivation subroutine solves the following regularized least-squares problem in parity space to obtain the initial attribution of the parity innovations to the bias vector $\alpha \in \mathbb{R}^6$.

$$\hat{\alpha}[k] = \arg\min_{\alpha} \|e_{\mathrm{ui}}[k] - D_b[k]\alpha\|_2^2 + \varepsilon_\alpha\|\alpha\|_2^2, \quad \varepsilon_\alpha > 0, \quad (25)$$

and with $J_{\mathrm{ls}}[k] = D_b[k]^\top D_b[k] + \varepsilon_\alpha I_6$, we define the score

$$s_i[k] = \frac{\hat{\alpha}_i[k]^2}{\big(J_{\mathrm{ls}}[k]^{-1}\big)_{ii}}. \quad (26)$$

We map $s_i[k]$ to an activation level using

$$\gamma_i[k] = \frac{1}{1 + \exp\big(-\alpha_\gamma(s_i[k] - s_{\mathrm{thr}})\big)}, \quad (27)$$

where $\alpha_\gamma > 0$ and $s_{\mathrm{thr}} > 0$ are tuning constants.

With $Q_b(\xi) = \mathrm{diag}(q_{\mathrm{bar}} \circ \exp(\xi))$ and $\Sigma_e(\xi)$ defined as above, we form the following objective function:

$$\begin{aligned} f(\xi) = {} & \log\det\Sigma_e(\xi) + \mathrm{tr}\big(\Sigma_e(\xi)^{-1}C_0[k]\big) + \kappa_0\sum_{i=1}^{n_b}(1-\gamma_i[k])\,\xi_i^2 \\ & + \mu_{\mathrm{white}}\sum_{j=1}^{L}\big\|\Sigma_e(\xi)^{-1}C_j[k]\big\|_F^2 + \kappa_t\sum_{i=1}^{n_b}\gamma_i[k]\big(\xi_i - \xi_{\mathrm{prev},i}\big)^2 \\ & + \kappa_{\mathrm{tie}}\sum_{1\leq i<j\leq 6}\big(1-\max(\gamma_i[k],\gamma_j[k])\big)\rho_{ij}[k]^2\big(\xi_i - \xi_j\big)^2, \end{aligned} \quad (28)$$

The optimization problem “InflationOpt” computes $\xi[k] \in \mathbb{R}^{n_b}_{\geq 0}$, and hence $\lambda[k] = \exp(\xi[k])$, by minimizing (28). The first two terms encourage agreement between the modeled whitened-innovation covariance $\Sigma_e(\xi)$ and the empirical statistic $C_0[k]$, while the term weighted by μ_{white} penalizes lagged parity correlations over the window L so as to discourage nonwhite innovation behavior. To reduce sensitivity when the magnetometer-related regression Gram matrix becomes poorly conditioned, we employ activation-weighted regularization, including a shrinkage term weighted by κ_0, which keeps low-activation components near their nominal values $\xi_i = 0$, a temporal penalty weighted by κ_t that discourages abrupt variation along supported directions, and a tying term weighted by κ_{tie}, which discourages large separations between highly coherent bias directions. Accordingly, the adaptation is biased toward directions that are better excited and better separated by the available data, while remaining conservative in weakly supported or nearly collinear directions. This design does not guarantee identifiability, but it helps reduce ill-conditioned covariance updates in practice.

V. Simulation Results

The numerical study uses the nonlinear Container-175 model from the Marine Systems Simulator (MSS) toolbox [17]. The simulator is augmented with ECEF inertial navigation equations, an IMU/GNSS integration pipeline based on [3], and World Magnetic Model (WMM)-based magnetic-field measurements [18]. All attacks are injected additively at the sensor-output level according to (1).

A simultaneous multi-sensor attack scenario is considered. The vessel is initially stationary. A surge command is applied at $t = 10\,\text{s}$, followed by a turning command at $t = 110\,\text{s}$, when the speed is around $9\,\text{m/s}$. From $t = 15\,\text{s}$, the accelerometer and gyroscope channels are corrupted by persistent sinusoidal injections. The GNSS position channel is attacked by step-like ECEF biases at $t = 170\,\text{s}$ and $t = 340\,\text{s}$, applied only on the ECEF Y- and Z-axes. The magnetometer attack starts at $t = 25\,\text{s}$ as a componentwise saturating ramp, reaches the saturation levels $[2000, 800, 1600]^\top$, and then follows scheduled bias changes, including an oscillatory segment after $t = 240\,\text{s}$ and a first-axis oscillatory component after $t = 250\,\text{s}$. The adaptive layer parameters were fixed at $\varpi_v = 0.99$, $L = 10$, $\varpi_{\text{fim}} = 0.99$, $\varepsilon_\rho = 10^{-8}$, $\varepsilon_\alpha = 10^{-4}$, $\alpha_\gamma = 2.5$, $s_{\text{thr}} = 1.6$, $\mu_{\text{white}} = 0.05$, $\kappa_0 = 0.005$, $\kappa_t = 5$, and $\kappa_{\text{tie}} = 10$.

Figs. 1 and 2 show the integrity-loss estimation errors in the magnetometer and GNSS position channels. The adaptive filter reduces the magnetometer bias-error norm RMSE from 1.63×10^3 to 4.41×10^2, and reduces the GNSS bias-error norm RMSE from $5.02\,\text{m}$ to $1.41\,\text{m}$. The equal GNSS peak values in Table I are caused by the GNSS bias transition, which neither recursive estimator can remove. The RMSE values quantify the improvement in post-onset tracking.

The improved integrity-loss tracking also improves attitude estimation. The attitude-error norm RMSE decreases from 3.33° to 0.907°, and the peak attitude error decreases from 13.5° to 3.27°, as shown in Fig. 3. Fig. 4 shows that both filters preserve similar ECEF position accuracy; the adaptive filter has $0.040\,\text{m}$ RMSE compared with $0.032\,\text{m}$ for the baseline. Thus, in this scenario, the main benefit of the adaptive layer is substantially better integrity-loss tracking and attitude robustness, while maintaining a small position error.

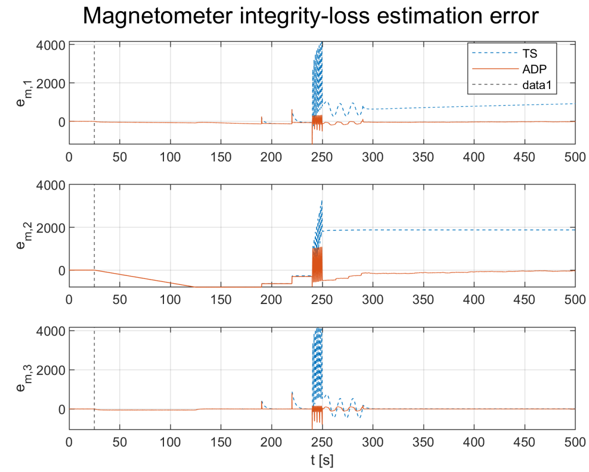

Fig. 1. Magnetometer integrity-loss estimation errors on the three axes.

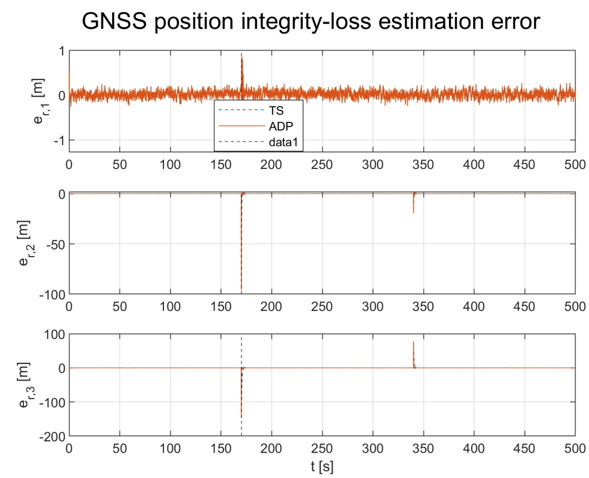

Fig. 2. GNSS position integrity-loss estimation errors on the three axes.

Fig. 5 reports the internal covariance-adaptation variables. The inflation factors increase mainly near attack-induced transients and along directions supported by the parity residuals, while the coherence indicators reveal weakly separable directions, especially in the magnetometer channel. This behavior is consistent with the activation- and coherence-aware regularization in (28) and explains why the adaptive filter improves bias tracking without inflating all channels.

VI. Concluding Remarks

This paper presented a loosely coupled marine PNT estimator for simultaneous integrity attacks on inertial, magnetic, and GNSS-position sensing. The estimator combines a descriptor unknown-input correction, which limits the influence of compromised IMU samples during the measurement update, with an adaptive two-stage bias layer to account for nonstationary GNSS position and magnetometer corruptions. In the simulated multi-sensor attack case, the adaptive filter

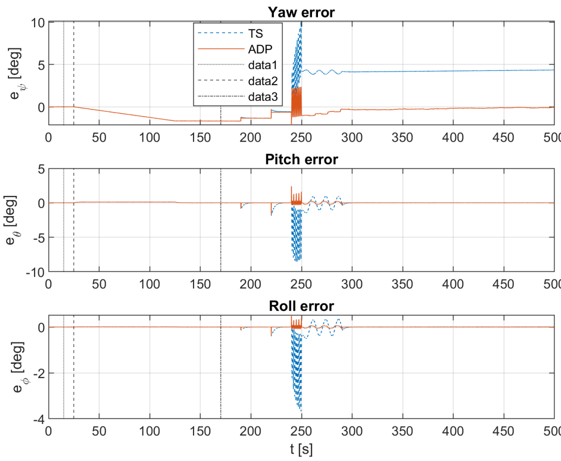

Fig. 3. Yaw, pitch, and roll estimation errors under the simultaneous attack scenario.

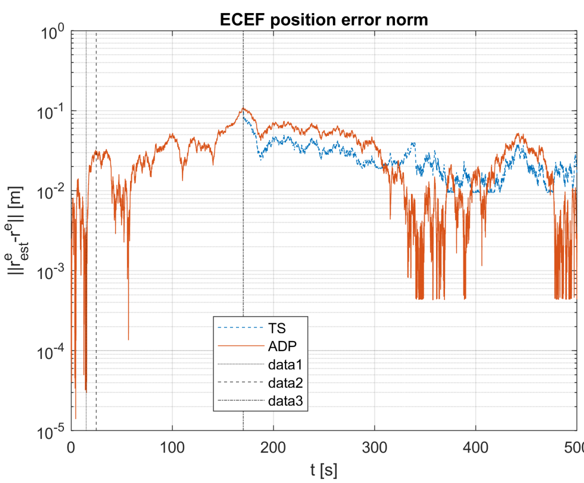

Fig. 4. ECEF position estimation error under simultaneous IMU, magnetometer, and GNSS attacks.

substantially reduced magnetometer and GNSS integrity-loss estimation errors and improved attitude estimation, while maintaining position accuracy under persistent sensor compromise. The results also indicate that the effectiveness of covariance adaptation depends on directional excitation and bias separability, particularly for magnetometer channels.

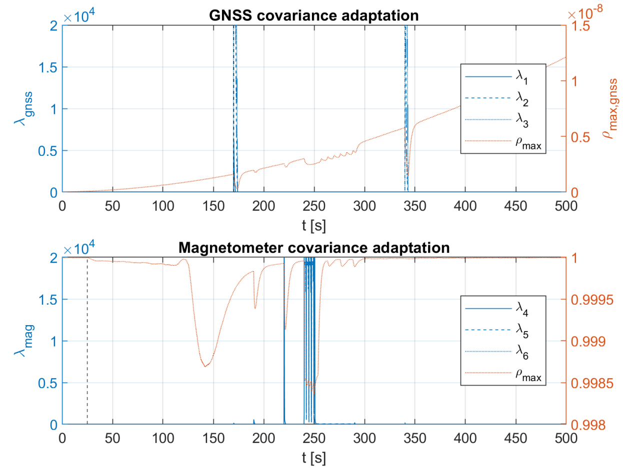

Fig. 5. Per-axis covariance inflation factors and maximum coherence indicators for the GNSS and magnetometer channels.

TABLE I

ERROR METRICS FOR THE ADAPTIVE FILTER (ADP) AND NON-ADAPTIVE TWO-STAGE BASELINE (TS)

Metric	RMSE (TS)	RMSE (ADP)	Peak (TS)	Peak (ADP)
Position error norm (m)	0.0324	0.0403	0.109	0.110
Attitude error norm (deg)	3.33	0.907	13.5	3.27
Mag. bias error norm	1.63×10^3	441	6.70×10^3	1.75×10^3
GNSS bias error norm (m)	5.02	1.41	175	175

REFERENCES

[1] C. Hemminghaus, J. Bauer, and E. Padilla, "BRAT: A BRidge attack tool for cyber security assessments of maritime systems," *TransNav: International Journal on Marine Navigation and Safety of Sea Transportation*, vol. 15, no. 1, 2021.

[2] U.S. Department of Transportation, "Positioning, navigation, and timing (pnt) strategic plan," tech. rep., U.S. DOT, 2025.

[3] P. D. Groves, "Principles of gnss, inertial, and multisensor integrated navigation system," *Artech House*, 2013.

[4] M. Taheri, M. Nematollahi, and K. Khorasani, "Detection and identification of gnss spoofing cyber-attacks for naval marine vessels," in *2023 IEEE International Symposium on Inertial Sensors and Systems (INERTIAL)*, pp. 1–4, IEEE, 2023.

[5] Q. Zhang, S. Luo, Z. M. Mao, M. Pajic, and M. K. Reiter, "Sok: How sensor attacks disrupt autonomous vehicles: An end-to-end analysis, challenges, and missed threats," *arXiv preprint arXiv:2509.11120*, 2025.

[6] J. H. Jung and J. W. Yoon, "Neutralization of imu-based gps spoofing detection using external imu sensor and feedback methodology," *arXiv preprint arXiv:2512.20964*, 2025.

[7] H. Meng, S. Luo, Z. Liang, Q. Huang, A. Khazraei, and M. Pajic, "Mars: Defending unmanned aerial vehicles from attacks on inertial sensors with model-based anomaly detection and recovery," *arXiv preprint arXiv:2505.00924*, 2025.

[8] S. Lee, "Gyro-mag: Attack-resilient system based on sensor estimation," *Sensors*, vol. 25, no. 7, p. 2208, 2025.

[9] D. Atmaca, C. de Visser, and E.-J. van Kampen, "Online inertial measurement unit fault identification and active fault-tolerant flight control," *Journal of Guidance, Control, and Dynamics*, vol. 48, no. 10, pp. 2389–2398, 2025.

[10] J. Keller and M. Darouach, "Two-stage estimator for dynamic stochastic systems subject to unknown inputs and random bias," in *1997 European Control Conference (ECC)*, pp. 255–260, IEEE, 1997.

[11] I. Giechaskiel and K. Rasmussen, "Taxonomy and challenges of out-of-band signal injection attacks and defenses," *IEEE Communications Surveys & Tutorials*, vol. 22, no. 1, pp. 645–670, 2019.

[12] Y. Jang, J. Park, J. Jung, *et al.*, "Paralyzing drones via emi signal injection on sensory communication channels," in *Network and Distributed System Security Symposium (NDSS)*, 2023.

[13] K. S. Tharayil, B. Farshteindiker, S. Eyal, N. Hasidim, R. Hershkovitz, S. Houri, I. Yoffe, M. Oren, and Y. Oren, "Sensor defense in-software (sdi): Practical software based detection of spoofing attacks on position sensors," *Engineering Applications of Artificial Intelligence*, vol. 95, p. 103904, 2020.

[14] C. Van Loan, "Computing integrals involving the matrix exponential," *IEEE transactions on automatic control*, vol. 23, no. 3, pp. 395–404, 2003.

[15] C.-S. Hsieh, "Robust two-stage kalman filters for systems with unknown inputs," *IEEE Transactions on Automatic Control*, vol. 45, no. 12, pp. 2374–2378, 2000.

[16] D. Zhou, Y. Su, Y. Xi, and Z.-J. Zhang, "Extension of friedland's separate-bias estimation to randomly time-varying bias of nonlinear systems," *IEEE Transactions on Automatic Control*, vol. 38, no. 8, pp. 1270–1273, 2002.

[17] T. Perez, O. Smogeli, T. Fossen, and A. J. Sorensen, "An overview of the marine systems simulator (mss): A simulink toolbox for marine control systems," *Modeling, identification and Control*, vol. 27, no. 4, pp. 259–275, 2006.

[18] NOAA NCEI Geomagnetic Modeling Team and British Geological Survey, "World magnetic model 2025," 2024.